ACS OMEGA

Open Access

http://pubs.acs.org/journal/acsodf

Article

Calcium Acetate Drug Produced from *Rapana venosa* Invasive Gastropod Shells: Green Process Control Assisted by Raman Technology

Danut-Alexandru Dumitru, Iuliana-Cornelia Poplacean, Karlo Maskaric, Tudor Tămaş, Lucian Barbu-Tudoran, and Simona Cinta Pinzaru*

Cite This: *ACS Omega* 2024, 9, 37086−37093

Read Online

ACCESS | Metrics & More | Article Recommendations | Supporting Information

ABSTRACT: The highly demanded calcium acetate ($Ca(CH_3COO)_2$) for biomedicine and various industries constantly requires green and low-cost methods of synthesis. In the present work, a sustainable approach to produce $Ca(CH_3COO)_2$ is reported as a proof of concept, processing for the first time as a starting material the worldwide highly abundant *Rapana venosa* shells, which is a neglected biogenic waste with high economical potential due to the rich mineral and organic pigmentary content. A green synthesis involving an eco-friendly acetic acid has been optimized at room temperature, without any additional energy consumption, and the resulting saturated $Ca(CH_3COO)_2$ solution was further slowly evaporated in three stages to obtain white $Ca(CH_3COO)_2$ crystalline powder, without impurity traces. Raman spectroscopy provided efficient structural information for every step of the process control, during demineralization as well as end product validation. Yields as high as 87.5% of highly pure $Ca(CH_3COO)_2$ mass have been achieved from raw *R. venosa* shells, proving the uniqueness and economic viability of the method. X-ray diffraction (XRD), scanning electron microscopy with energy-dispersive spectroscopy (SEM-EDX), and Fourier-Transform IR spectroscopy (FTIR) analyses validated the final product identity, hydration status, crystalline morphology, and composition. The purity of the resulting product suggests a high valorization potential of the abundant *R. venosa* shell in the context of the blue bioeconomy and offers a cleaner and efficient method of $Ca(CH_3COO)_2$ production with important applications in relevant industries.

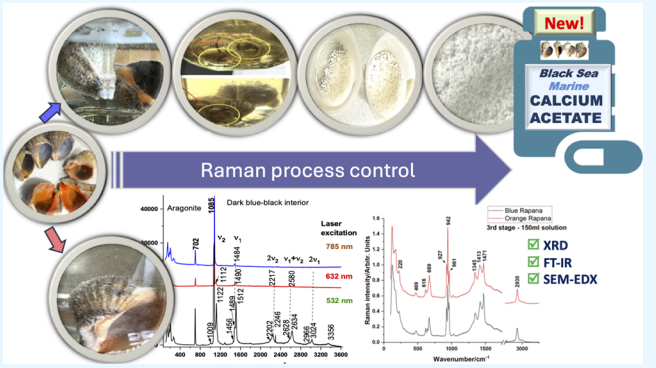

INTRODUCTION

The invasive spread of the *Rapana venosa* (Valenciennes, 1846) gastropod around the globe has been deeply studied and documented.[1,2] The most significant areas of invasion are the Black Sea[3] and the Adriatic Sea basins,[4] the North Sea,[5] Chesapeake Bay,[6] the Uruguayan and Argentinian coasts,[7] and its predatory characteristics and lack of direct competition induced negative impact over the invaded ecosystems. Due to its worldwide spread, large amounts of shells are brought ashore and discarded by fisheries and the seafood industry sector, as the meat is harvested for economic purposes, commonly getting stored in municipal waste centers where they contribute to air and soil pollution due to microbial decomposition.

The rich mineral content of marine shells is widely reported,[8−10] representing more than 90−95% calcium carbonate polymorphs, mainly calcite and aragonite.[11] Moreover, a complex organic biomatrix is also present, giving intricate colorations specific to the adaptation for the marine environment; the pigments are composed of valuable carotenoids and polyenes, which could be further extracted and processed.

The New Blue Economy concept regarding American ocean coasts and the European Union Commission agenda introduced the blue bioeconomy context[12] as an important and innovative action plan to overlook the nonregenerable land sources and develop novel pharmaceuticals, nutraceuticals, food additives, and livestock feeds from renewable marine derivates, which, in many cases, highlighted more significant advantages. By implementing objectives included in the ambitious plans, the significant issue of biogenic waste management could be dramatically minimized, as the

Received: April 30, 2024
Revised: August 9, 2024
Accepted: August 12, 2024
Published: August 21, 2024

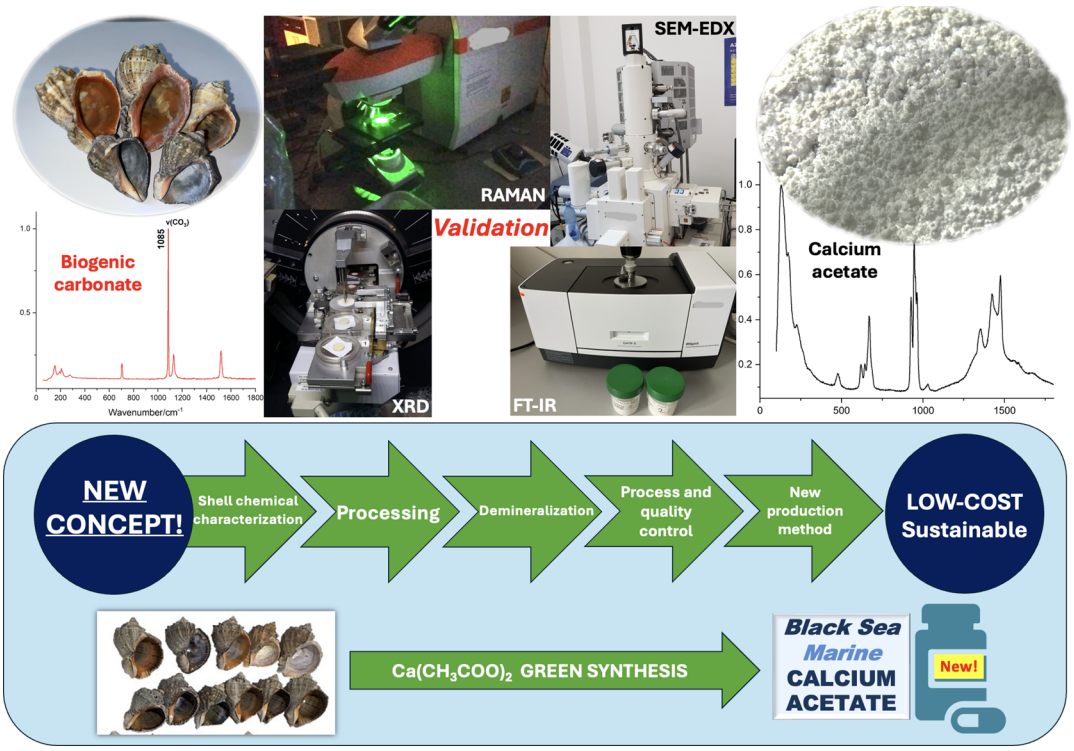

Figure 1. Graphical sketch illustrating the green process of reusing *Rapana venosa* raw shell waste to produce calcium acetate of a marine source.

preponderant content of $CaCO_3$ in marine shells makes their processing as raw materials relevant in the rapidly developing recycling economy. Although the seashells market sometimes includes spectacular snail species,[13] out of them many being protected by current regulations, it is not the case of *R. venosa*, due to its invasive character, rated among the worst 100 invasive species.[14]

$Ca(CH_3COO)_2$ is an inexpensive white crystalline powder of calcium salt, commonly synthesized from nonrenewable land derived sources of calcium carbonate, such as limestones, marble, or other carbonate rocks, which are soaked in concentrated solutions of acetic acid. This process implies several negative environmental effects given by the operation and exploitation of mines.[15−17]

A growing demand for $Ca(CH_3COO)_2$ by several industries is showcased due to its various specific applications. In the biomedical field, $Ca(CH_3COO)_2$ is administrated to patients with hyperphosphatemia from chronic kidney disease for its efficient and rapid phosphate binding characteristics.[18−20] Further, high solubility in water and slightly basic behavior in aqueous solutions make $Ca(CH_3COO)_2$ an important additive in the food industry as an acidity regulator.[21] It also acts as a filler agent for concrete fabrication, being added as a curing accelerator while also improving the strength and durability of this building materials.[22,23] In water treatment, this versatile acetic salt is used to remove potentially pollutant phosphate compounds from water, forming calcium phosphate precipitates.[24]

Increased industrial applications will require an easy, low-cost, and environmentally sustainable synthetization approach for raw materials. Green methods of $Ca(CH_3COO)_2$ production using eggshells[25] or oyster shells[26,27] were extensively discussed, resulting in the most common monohydrate form. Thus, exploring the possibility of processing *R. venosa* biomass for $Ca(CH_3COO)_2$ production becomes a highly relevant topic, due to its worldwide invasion and lack of references on shell morpho-chemical structure, which could potentially lead to better invasion management and decrease in coastal biogenic waste. This approach will not require energy consumption in the demineralization process, as the shells are processed intact, which could also be proven economically viable.

In the present work, an eco-friendly chemical approach is developed for the smart reuse of the *R. venosa* gastropod shell waste without grinding, powdering, or other energy-consumption process, for the effective production of high-quality calcium acetate, marking this study as the first report of the valorization method for this specific and abundant biogenic material. The morpho-chemical characteristics of the product are demonstrated using Raman technology, which is suitable for entire process control from raw waste to final product and validated by complementary techniques such as Fourier-transform infrared spectroscopy (FTIR), X-ray diffraction (XRD), and scanning electron microscopy with energy-dispersive spectroscopy (SEM-EDX), as well as the elemental analysis. Our preliminary investigations on this species[28] indicated that the $Ca(CH_3COO)_2$ quality from gastropod shells is superior to that resulting from crustaceans demineralization and deserves more analytical attention due to its potential for the upscaled process of economic importance.

MATERIALS AND METHODS

R. venosa specimens were collected from the Romanian coasts of the Black Sea, from a touristic beach near the city of Năvodari (44°18′07.4″ N, 28°37′38.4″ E) during December 2023. Three specimens were randomly selected from the statistically relevant collected stock of shells featuring different pigmentation. Intense orange-pink and blue dominant pigmented shells were separately treated since the different

https://doi.org/10.1021/acsomega.4c04138
ACS Omega 2024, 9, 37086−37093

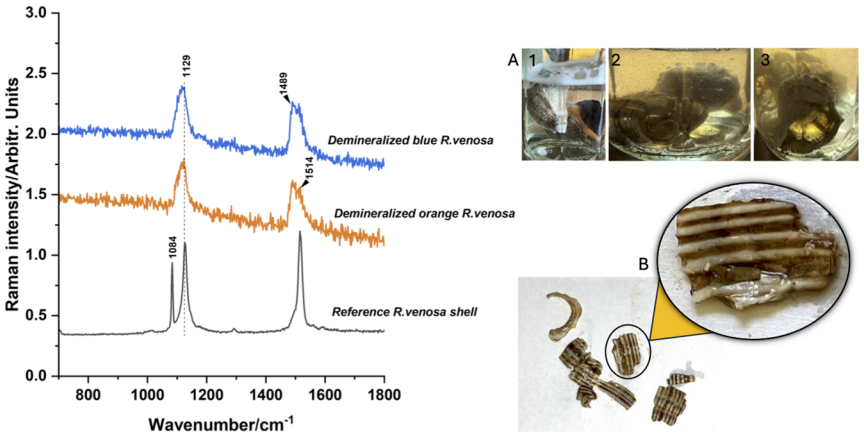

Figure 2. Raman spectra of starting material (*Rapana venosa* raw shells) and of the soft fragments detached during demineralization process control after 14 days in acetic acid bath, for both orange and blue pigmented shells, as indicated in each spectrum. Photos of the (A) (1) blue *Rapana venosa* specimens during demineralization, and after 14 days of treatment are showed in inset; (2) lateral view and (3) ventral view; (B) Detached demineralized organic layer details showing soft fragment featuring a strip pattern of light-dark brown appearances and responsible for the characteristic Raman signal of two broaden bands, at 1120 and between 1489 and 1514 cm^{-1}, under 532 nm excitation.

pigmentation may induce different chemical behaviors within the demineralization approach. Before immersing the entire shells in a demineralization bath of 9% acetic acid solution, a cleaning process for the removal of soft tissue residues and other attached sand or debris has been carefully conducted. Two separate glass containers, each comprising 180 mL of a 9% acetic acid solution, were prepared. The first container accommodated a sizable *R. venosa* shell with a vivid orange pigmentation (as illustrated in Figure 1), weighing 25.6 g, while in the second container, two shells exhibiting blue interior pigmentation, with a cumulative mass of 28 g, were immersed.

The demineralization process was held under constant monitoring for 2 weeks at room temperature until the achievement of $Ca(CH_3COO)_2$ solution saturation. Solid detached shell residues comprising organic counterparts were filtered using slow flow rate (25 mL/min) paper filters, and the final $Ca(CH_3COO)_2$ solutions were slowly heated below 40 °C using hot plates in three volumetric stages to obtain an accurate quantitative evaluation on the yielded solid $Ca(CH_3COO)_2$ crystals. Initially, 1 mL of each solution was subjected to evaporation from the respective sample and denoted from now on calcium acetate from orange (CAO) and blue (CAB) shells. Next, 30 mL of solution from each sample was subject to a second crystallizing process, resulting in the second batch of products (CAO 30 mL, CAB 30 mL), and finally, the leftover volume of demineralization solutions underwent the same procedure to result the third batch of products (CAO 149 mL, CAB 149 mL), thus, three distinct batches of synthesized $Ca(CH_3COO)_2$ being independently obtained during the demineralization process, which allowed to conclude on the eventual difference among process steps and timing.

Independently, a control product consisting of a geogenic $Ca(CH_3COO)_2$ was synthesized, by dissolving 1 g of standard geogenic $CaCO_3$ (CAS 471-34-1, > 99% purity) in 5 mL aqueous solution of 11% acetic acid. The resulting mixture was stirred magnetically at a controlled temperature for 60 min, evaporated, and subsequently resulted white, crystalline powders were dried in an oven at 60 °C for 24 h.

Elemental analysis of the $Ca(CH_3COO)_2$ samples was carried out using a Thermo Flash EA 1112 CHN analyzer.

Raman spectra acquisition was performed on the raw waste shells to check their corresponding calcite-aragonite conformity, then during the process, to verify the decrease of the carbonate signal along the demineralization progress, and the three batches of the resulted $Ca(CH_3COO)_2$ crystals products, using a Renishaw InVia Confocal Raman system, employing a 785 nm diode laser line excitation, having the nominal power of 300 mW and equipped with one Vis/NIR optical objective of 20x, Spectra were collected with 1 cm^{-1} spectral resolution, and the parameters were optimized in Wire 3.4 acquisition software. For calibration, an internal silicon wafer was employed.

XRD patterns of the resulted crystalline batches were recorded using a Bruker D8 Advance diffractometer in Bragg−Brentano geometry, with a Cu tube with λ = 0.15418 nm, Ni filter, and a Lynx Eye detector. Corundum (NIST SRM1976a) is used as an internal standard. The data were collected on a 5−70° 2θ interval at a 0.02° 2θ step, with each step measured for 0.5 s. The identification of mineral phases was performed with the Diffrac Eva 2.1 software (Bruker AXS) using the PDF2 (2012) database.

A Shimadzu FTIR IRSPIRIT with a QATR-S accessory, holding a single-reflection integration-type ATR module with a diamond prism, has been used to record the FTIR spectra of the biogenic $Ca(CH_3COO)_2$ batches in the 650−4000 cm^{-1} spectral range, performing 80 accumulations per spectrum with 4 cm^{-1} spectral resolution.

SEM-EDX imaging was carried out using a SU8230 Hitachi ultrahigh resolution cold-field emission scanning electron microscope. This instrument enables the acquisition of both topographical and compositional information with a feature resolution of up to 1 nm under optimal conditions. Prior to analysis, samples were securely affixed to SEM holders from Hitachi, which consisted of aluminum holders with M4 threads covered by 3 mm thick carbon discs. Additionally, a Quorum Q150T sputtering sample coater, capable of controlled gold sputtering with a thickness of 10 nm (density 19.32 g/m^3) at a rate of 14 nm/min, was utilized in the process.

The resulting data set was subjected to extensive processing and analysis using the OriginPro 2024 software package from Originlab Corporation, Northampton, Massachusetts, USA.

https://doi.org/10.1021/acsomega.4c04138
ACS Omega 2024, 9, 37086−37093

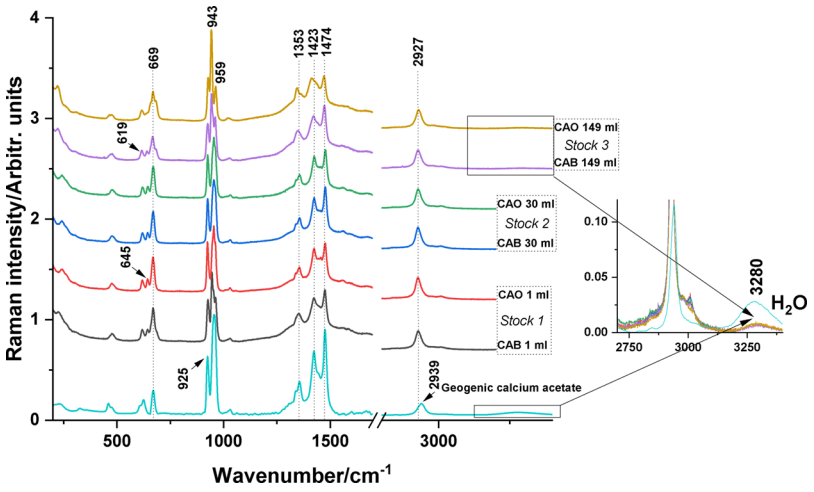

Figure 3. Raman spectra of resulted $Ca(CH_3COO)_2$ crystalline powder from three batches from the demineralization bath along the process, denoted as stock 1, 2, and 3, as indicated. Crystals exhibited coexisting hydration states, featuring vibrational peaks of $Ca(CH_3COO)_2{\cdot}H_2O$ and $Ca(CH_3COO)_2{\cdot}0.5H_2O$, with shared spectral signatures indicating varying hydration levels, as shown in the zoom of the water bands range. Rapid evaporation favored lower hydration forms, while slower evaporation resulted in the dominance of the monohydrate salt, as indicated by Raman peaks.

RESULTS AND DISCUSSION

Prominent signs of demineralization have been displayed on the *R. venosa* shells after 2 weeks of immersion in the CH_3COOH aqueous solution and illustrated in Figure 2A, evident through an intensive shell interior depigmentation, appearance of through holes, and exterior side shell layer detachment, which indicated important characteristics of the gastropod shell morphology, such as the absence of a homogeneous organic layer used by marine specimens for mineral scaffold development. In addition, the detachment of exterior brown patterned soft fragments indicated a clear organic layer separation from the outer shell surface. Since the organic composition of the *R. venosa* shell species is not reported, this process provided robust support information for further devoting dedicated study in understanding the organic tiny and intricate distribution within the mineral dominant composition.

The Raman spectra were acquired on detached shell fragments of soft consistency, as seen in Figure 2B, after 14 days of acetic acid immersion using 785 nm nonresonant excitation confirming the expected absence of the ∼1085 cm^{-1} ($\nu_1(CO_3^{-2})$ symmetric stretching mode of calcium carbonate mineral, thus, indicating is dissolution (Figure 2). The only present component of the *R. venosa* shell after demineralization comes from the organic biomatrix, composed of a combination of unsubstituted polyenes, with vibrational bands visible at 1129 cm^{-1} (ν_2(C−C) stretching mode), and 1489−1515 cm^{-1} (ν_1(C═C) stretching mode), suggesting that after the $CaCO_3$ dissolution reaction with CH_3COOH for the sustainable production of $Ca(CH_3COO)_2$, the byproduct consists in an insoluble organic component, rich in pigments, which could be further utilized, making important steps in achieving complete biogenic shell waste valorization.

The absence of main $\nu_1(CO_3^{-2})$ is noted from samples undergoing demineralization and highly fluorescent behavior is highlighted, indicating successful $CaCO_3$ extraction in reaction with the 9% CH_3COOH solution. The visual appearance of the shells after 14 days in the demineralization bath is shown in Figure 2, where detached soft layer fragments consisting of organic leftovers are highlighted for two samples, the orange pigmented specimen (CAO), and the blue pigmented shells (CAB). The observed Raman bands from the stripped light-dark brown alternance pattern appearance (Figure 2) indicated two broadened bands, at 1120 and between 1489 and 1514 cm^{-1}, under 532 nm excitation. These bands are characteristic to polyene pigments and suggest multiple contributions. Since the pigments of this shell species and their different coloration are yet unstudied, a dedicated study on this aspect will be addressed in more detail elsewhere.

As the green demineralization process did not require additional energy consumption and gastropod shells were processed intact, this method of synthesis becomes important due to its economic viability. The resulting $Ca(CH_3COO)_2$ yield was observed as higher in the CAB samples, specifically 87.5%, whereas the CAO sample highlighted 72.2% yield, thus 15.3% lower.

Raman spectroscopy was the main analytical tool used to qualitatively assess the resulted $Ca(CH_3COO)_2$ crystals after each evaporation step of the three batches (1, 30, 149 mL), and the results were compared with Raman spectra of geogenic $Ca(CH_3COO)_2$ in order to highlight any modifications in peak position or intensity, as showed in Figure 3.

Each sample of the resulting crystals revealed the coexistence of two degrees of hydration specific for $Ca(CH_3COO)_2$, with vibrational peaks of $Ca(CH_3COO)_2{\cdot}H_2O$ and $Ca(CH_3COO)_2{\cdot}0.5H_2O$. In all acquired spectra, vibrational peaks shared between the two forms are observed at ∼476 cm^{-1} ρ_{ip}(OCO) (in plane bending of acetate anion), ν_{as}(C═C) (asymmetric C−O stretching in acetate) being split in two bands at 1560 and 1600 cm^{-1}, 1673 cm^{-1} ν(C═O) (stretching of carbonyl), and the methyl group's symmetric and asymmetric stretching vibrations ($\nu_s(CH_3)$ and $\nu_{as}(CH_3)$) at 2928 and 3009 cm^{-1}.[29]

Furthermore, the four samples, two from the first (1 mL) and two from the second batch (30 mL), respectively (CAO 1 mL, CAO 30 mL, CAB 1 mL, CAB 30 mL) showed a higher half-hydrate concentration presence as revealed by the Raman bands at 619, 644 cm^{-1} ρ_{op}(OCO) (out of plane OCO bending), 669 cm^{-1} δ_s(OCO) and δ(OCO) (symmetric OCO bending and twisting), 925, 947, 954, and 960 cm^{-1} ν(C−C)

https://doi.org/10.1021/acsomega.4c04138
ACS Omega 2024, 9, 37086−37093

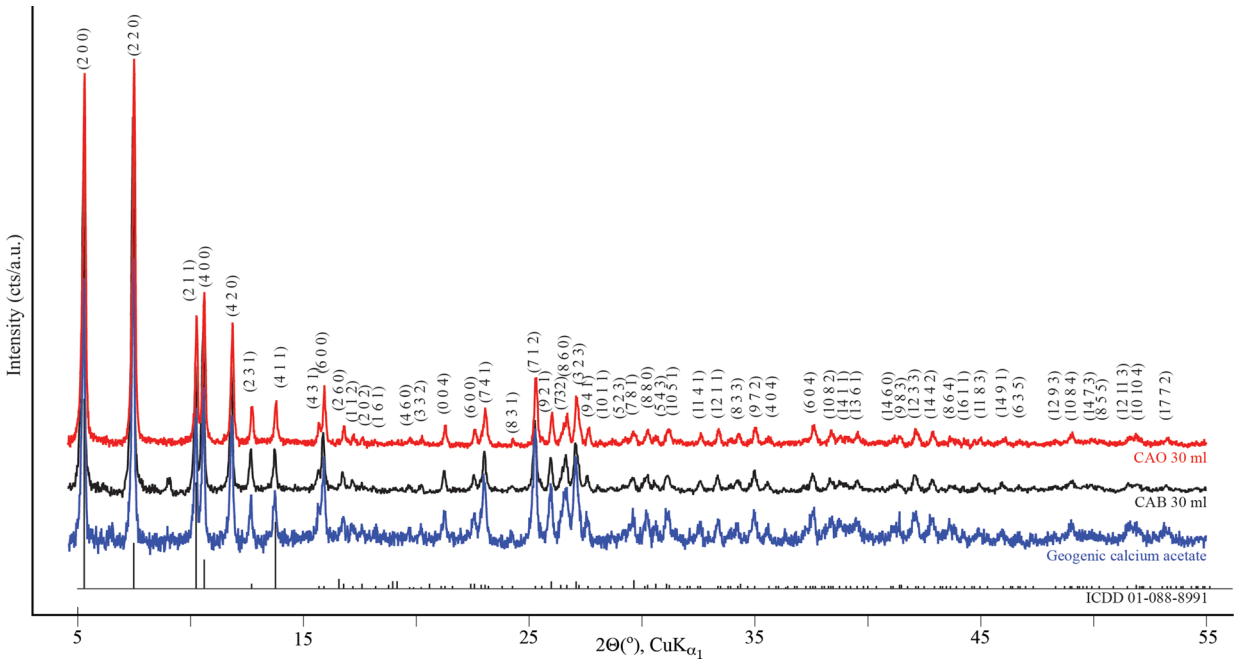

Figure 4. Measured X-ray diffractograms of calcium acetate samples obtained from the second batch of volumetric evaporation of bathing solution (CAO 30 mL and CAB 30 mL), with specific diffraction peaks of Ca(CH3COO)2·0.5H2O and low intensity peaks of $Ca(CH_3COO)_2{\cdot}H_2O$ in CAB 30 mL samples. The PDF 01-088-8991 pattern is shown as a comparison.

(C−C stretching in acetate anion), 1338, and 1353 cm^{-1} $\delta_s(CH_3)$ (symmetric bending of methyl group), 1423 cm^{-1} $\delta_{as}(CH_3)$ (asymmetric bending of methyl group), and 1475 cm^{-1} $\nu_{as}(CO)$ (asymmetric stretching of acetate). The third batch (CAO 149 mL, CAB 149 mL) clearly indicated a monohydrate $Ca(CH_3COO)_2$ dominance with peaks at 641 cm^{-1} $\rho_{op}(OCO)$, 685 cm^{-1} $\delta_s(OCO)$ and $\delta(OCO)$, 928, and 943 cm^{-1} $\nu(C-C)$, 1347 cm^{-1} $\delta_s(CH_3)$, 1413 cm^{-1} $\delta_{as}(CH_3)$, and 1472 cm^{-1} $\nu_{as}(CO)$.

As preliminary information, a similar synthesis from *R. venosa* shell randomly selected from the shore was previously performed to offer an overview in comparison with the $Ca(CH_3COO)_2$ byproduct resulted from demineralization of a crustacean species, specifically *Callinectes sapidus*, to produce transparent polymer foils.[28] Here, Raman spectroscopy results also indicated that the low volume of evaporated aqueous solution produced hemihydrate dominant $Ca(CH_3COO)_2$ crystalline powder with vibrational spectra similar to that of geogenic $Ca(CH_3COO)_2$, while the byproduct produced from the blue crab appeared as a mixture of monohydrate form and calcium hydrogen acetate. The current results regarding the hydration status of the obtained calcium acetate from the present shell stock are consistent with the preliminary data.[28]

Although the first four samples (CAO 1 mL, CAO 30, CAB 1, and CAB 30 mL) appear to be $Ca(CH_3COO)_2{\cdot}0.5H_2O$ dominant, low intensity bands of $Ca(CH_3COO)_2{\cdot}H_2O$ from 945 and 1474 cm^{-1} are still visible in their respective Raman spectra. Similarly, in the third, upscaled batch (CAO 149 mL, CAB 149 mL), weak bands of $Ca(CH_3COO)_2{\cdot}0.5H_2O$, specifically 617, 667, 926, 950, 960, and 1421 cm^{-1} are present, suggesting a coexistence, but rather in variable concentrations, which could be explained due to the difference in the evaporation rates given by the different volumes of $Ca(CH_3COO)_2$ aqueous solution. The rapid evaporation rate of 1 and 30 mL samples led to crystal formation of a lower degree of hydration of $Ca(CH_3COO)_2$, which shares a H_2O molecule between the $Ca(CH_3COO)_2$ molecules in the crystalline structure, when the slow evaporation process of 149 mL solution samples led to the favored formation of the monohydrate salt.

Elemental analysis % calcd. found for $Ca(CH_3COO)_2$ monohydrate, $C_4H_8O_5Ca$ (MW 176 181 g/mol): C 27.27% (27.17%); H 4.58% (4.34%).

FTIR spectra (Figure S1 from the Supporting Information) were acquired on $Ca(CH_3COO)_2$ crystals resulting at each evaporation step. The vibrational signal specific to the $Ca(CH_3COO)_2$ anion is observed with vibrational bands at 618 and 670 cm^{-1} $\rho_{op}(OCO)$, 943 cm^{-1} $\nu(C-C)$, 1024 cm^{-1} $\rho_{op}(CH_3)$, 1412 and 1452 cm^{-1} $\nu_s(C-O)$, and 1540 cm^{-1} $\nu_{as}(C-O)$. Additionally, from the third batch (CAO 149 mL and CAB 149 mL) solid samples resulted after the last stage of evaporation, a broad FTIR band in the 2840−3670 cm^{-1} range becomes visible due to $\nu_s(OH)$ and $\nu_{as}(OH)$ stretching vibrations of H_2O molecule offering a clear indication on the degree of hydration of the $Ca(CH_3COO)_2$ crystals. Furthermore, while this feature is missing from the FTIR spectra of CAO 1 mL, CAO 30, CAB 1, and CAB 30 mL, a higher concentration of low hydrated $Ca(CH_3COO)_2$, mainly $Ca(CH_3COO)_2{\cdot}0.5H_2O$, is present in the first batch of samples.

XRD patterns are showcased in Figure 4 and were acquired from the second-stage samples where 30 mL of $Ca(CH_3COO)_2$ solution was evaporated (CAO 30 mL and CAB 30 mL). The synthesized geogenic $Ca(CH_3COO)_2$ produced as reference material is composed only of the $Ca(CH_3COO)_2{\cdot}0.5H_2O$ form. The common peaks in the diffractograms obtained from the *R. venosa* derived $Ca(CH_3COO)_2$ indicate a dominant presence of the tetragonal hemihydrate form in both orange and blue patterned shell samples analyzed, fairly similar to both PDF cards 00-019-0199[30] and 01-088-8991.[31] In the case of the CAB 30 mL sample, diffraction peaks at 2θ = 9.02 and 23.5° were assigned to the monohydrate form based on PDF 00-019-0200 and data

https://doi.org/10.1021/acsomega.4c04138
ACS Omega 2024, 9, 37086−37093

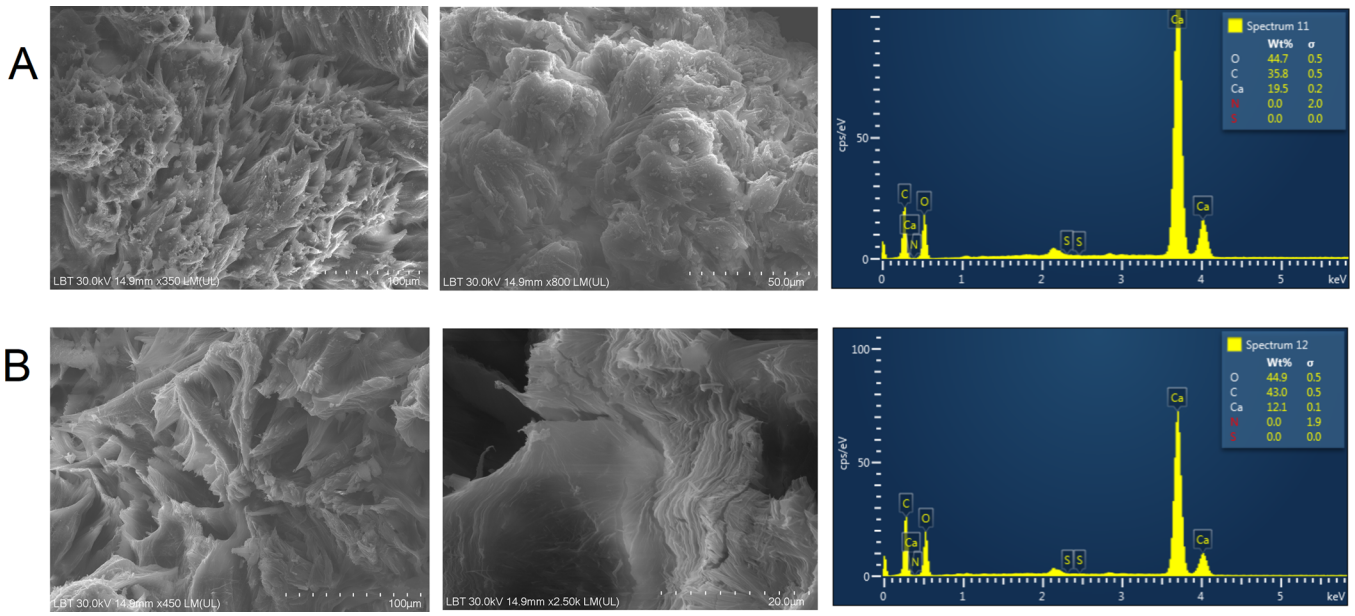

Figure 5. SEM-EDX images of CA samples resulted after the second stage of evaporation, (A) CAO 30 mL and (B) CAB 30 mL, showing intricate acetate crystals ultramorphology of compact rough microconglomerates. Energetic bands from CA are present in the EDX spectra with a minimal signal from impurities.

from Bette et al.[32] in very low concentrations, observation sustained by Raman spectroscopy results.

As per resulted diffraction patterns and considering the well-correlated results from Raman and FTIR analyses which totally revoke the presence of any other polysaccharides or proteins, only highly crystalline $Ca(CH_3COO)_2$ was obtained as a high-quality product by immersing intact *R. venosa* shells in a CH_3COOH low concentrated bath.

The SEM images of $Ca(CH_3COO)_2$ crystals reveal particular aspects of their specific ultrastructure. Crystals resulted from the *R. venosa* derived solution have both compact spiky and microboulder conglomerate morphology (Figure 5A,B).

Calcium acetate samples from both orange and blue pigmented shells presented similar elemental composition, as revealed by EDX, consisting of Ca, C, and O, with considerably small traces of nitrogen (<0.1 wt %). The lack of any inorganic impurities, which tend to appear in the final product in industry due to the use of limestones as raw materials and often require further processing to be removed, strongly suggests that employing *R. venosa* shells as a main source of calcium carbonate leads to the production of $Ca(CH_3COO)_2$ crystals with the highest degree of purity.

CONCLUSIONS

The present study demonstrates for the first time the potential utilization of *R. venosa* shells as a primary source of calcium carbonate to produce $Ca(CH_3COO)_2$, with specific applications in the biomedical industry. The demineralization process of the biogenic material in CH_3COOH solution immersion was carefully monitored over a 14 day period, resulting in shell degradation, calcium carbonate dissolution, and subsequently, efficient recovery of $Ca(CH_3COO)_2$ white crystalline powder from demineralization bath solution.

Spectral analysis using Raman spectroscopy, FTIR, and XRD revealed the formation of highly pure $Ca(CH_3COO)_2$ crystals following induced evaporation. SEM-EDX results further demonstrated the production of compact conglomerates of calcium acetate with minimal impurities.

The idea of using waste biological material for calcium acetate preparation is to relieve pressure from conventional methods of calcium acetate production, which are based on limited resources and are energy intensive. In that regard, using biological waste material as a source for calcium acetate production reduces cost and environmental impact in comparison with conventional methods of using limestones or other calcium-carbonated rocks. Previous studies reported different maximum yields of calcium acetate using different waste biological materials and optimizing the preparation process, in particular acetic acid solution concentration.[25−27] Calcium acetate obtained from eggshells had a maximum experimental yield of 96.5% with 100% acetic acid theoretical concentration; from scallops, it was 87.05% using 60% acetic acid concentration, and from oyster shells, it had a maximum yield of 93% with 68.91% acetic acid concentration. In comparison, we used a less concentrated acetic acid solution (9%) and achieved a maximum yield of 87.5%.

Utilizing *R. venosa* waste shells in the presented process aligns with the goals of the blue bioeconomy agenda, facilitating the recycling and valorization of otherwise discarded marine waste commonly deposited in municipal centers. This approach represents a promising step toward sustainable resource utilization and environmental conservation efforts.

Green, sustainable, efficient, and high-quality production of calcium acetate from waste shells of aragonite-calcite mineral polymorphs is demonstrated, and a new product proposed as "marine calcium acetate" would be of high demand for pharmaceutical, food, and cosmetics industries as well for the biomedical field.

https://doi.org/10.1021/acsomega.4c04138
ACS Omega 2024, 9, 37086−37093

■ ASSOCIATED CONTENT

Supporting Information

The Supporting Information is available free of charge at https://pubs.acs.org/doi/10.1021/acsomega.4c04138.

Comparative FTIR spectra between CAO and CAB crystals samples (PDF)

■ AUTHOR INFORMATION

Corresponding Author

Simona Cinta Pinzaru − *Ioan Ursu Institute of the Faculty of Physics, Babeş-Bolyai University, 400084 Cluj-Napoca, Romania; RDI Institute in Applied Natural Sciences, 400327 Cluj-Napoca, Romania;* orcid.org/0000-0001-8016-4408; Email: simona.pinzaru@ubbcluj.ro

Authors

Danut-Alexandru Dumitru − *Ioan Ursu Institute of the Faculty of Physics, Babeş-Bolyai University, 400084 Cluj-Napoca, Romania;* orcid.org/0000-0001-8078-2775

Iuliana-Cornelia Poplacean − *Ioan Ursu Institute of the Faculty of Physics, Babeş-Bolyai University, 400084 Cluj-Napoca, Romania*

Karlo Maskaric − *Ioan Ursu Institute of the Faculty of Physics, Babeş-Bolyai University, 400084 Cluj-Napoca, Romania; RDI Institute in Applied Natural Sciences, 400327 Cluj-Napoca, Romania*

Tudor Tămaş − *Department of Geology, Babeş-Bolyai University, 400084 Cluj-Napoca, Romania*

Lucian Barbu-Tudoran − *Electron Microscopy Center, Department of Experimental Biology, Babeş-Bolyai University, 400006 Cluj-Napoca, Romania*

Complete contact information is available at: https://pubs.acs.org/10.1021/acsomega.4c04138

Author Contributions

Conceptualization: D.-A.D., S.C.P.; methodology: D.-A.D., I.-C.P., K.M., and S.C.P.; validation: D.-A.D., I.-C.P., K.M., T.-L.T., and S.C.P.; investigation: D.-A.D., I.-C.P., K.M., T.-L.T., S.C.P., and L.B.-T.; resources: D.-A.D., S.C.P.; data curation: D.-A.D.; writing, review, and editing: D-A.D., I.-C.P., T.-L.T., and S.C.P.; supervision: S.C.P. All authors have given approval to the final version of the manuscript.

Notes

The authors declare no competing financial interest.

■ ACKNOWLEDGMENTS

The authors thank professor Emese Gál from the Faculty of Chemistry and Chemical Engineering, Babes-Bolyai University, for elemental analysis.

■ ABBREVIATIONS

CA, calcium acetate; XRD, X-ray diffraction; SEM-EDX, scanning electron microscopy coupled with energy-dispersive X-ray spectroscopy; FTIR, Fourier-transform IR spectroscopy

■ REFERENCES

(1) Xue, D. X.; Graves, J.; Carranza, A.; Sylantyev, S.; Snigirov, S.; Zhang, T.; Liu, J. X. Successful Worldwide Invasion of the Veined Rapa Whelk, Rapana Venosa, despite a Dramatic Genetic Bottleneck. *Biol. Invasions* **2018**, *20* (11), 3297−3314.

(2) Mann, R.; Occhipinti, A.; Harding, J. M. *Alien Species Alert: Rapana Venosa (Veined Whelk)*; ICES Cooperative Research Reports (CRR), 2004.

(3) Dağtekin, M. The Invasive Mollusk Rapana Venosa (Mollusca: Neogastropoda: Muricidae) in the Mid-Southern Black Sea: Distribution, Growth, and Stock Structure. *Acta Ichthyol. Piscat.* **2023**, *2023* (53), 191−199.

(4) Savini, D.; Occhipinti-Ambrogi, A. Consumption Rates and Prey Preference of the Invasive Gastropod Rapana Venosa in the Northern Adriatic Sea. *Helgol Mar Res.* **2006**, *60* (2), 153−159.

(5) Dennis, C. N.; Johannes, N. J. P.; Robert, J. V. Rapana Venosa (Gastropoda: Muricidae): A New Invasive Species in the North Sea. *Deinsea* **2005**, *11* (1), 169−174.

(6) Mann, R.; Harding, J. M. *Salinity Tolerance of Larval Rapana Venosa: Implications for Dispersal and Establishment of an Invading Predatory Gastropod on the North American Atlantic Coast*; 2003; Vol. *204*. http://www.jstor.orgURL:http://www.jstor.org/stable/1543499Accessed:25-12-201509:28UTC.

(7) Giberto, D. A.; Bremec, C. S.; Schejter, L.; Schiariti, A.; Mianzan, H.; Acha, E. M. The Invasive Rapa Whelk Rapana Venosa (Valenciennes 1846): Status and Potential Ecological Impacts in the Río de La Plata Estuary, Argentina-Uruguay. *J. Shellfish Res.* **2006**, *25* (3), 919−924.

(8) Wardiatno, Y.; Riyanto, B.; Iskandar, N. A.; Kleinertz, S.; Funch, P.; Kurniawan, F. A New Marine Biomaterial: The Shell of Mangrove Horseshoe Crabs, Carcinoscorpius Rotundicauda (Latreille, 1802) Emphasizing Its Physico-Chemical Characteristics. *Front. Mar. Sci.* **2021**, *8*, No. 612016.

(9) Wan, M.-C.; Qin, W.; Lei, C.; Li, Q.; Meng, M.; Fang, M.; Song, W.; Chen, J. Hua; Tay, F.; Niu, L.-N. Biomaterials from the Sea: Future Building Blocks for Biomedical Applications. *Bioact. Mater.* **2021**, *6*, 4255−4285.

(10) Hou, Y.; Shavandi, A.; Carne, A.; Bekhit, A. A.; Ng, T. B.; Cheung, R. C. F.; Bekhit, A. E. D. A. Marine Shells: Potential Opportunities for Extraction of Functional and Health-Promoting Materials. *Crit Rev. Environ. Sci. Technol.* **2016**, *46* (11−12), 1047−1116.

(11) Podaralla, N. K.; Paramasivam, P.; Jacquemin, J. Characterization of Hydrothermally Decomposed and Synthesized CaCO3 Reinforcement from Dead Snail Shells. *ACS Omega* **2024**, *9* (2), 2183−2191.

(12) European Commission; DG MARE - DG for Maritime Affairs and Fisheries. *Blue Bio-Economy − Situation Report and Perspectives*; Publications Office of the European Union, 2018.

(13) Nijman, V.; Spaan, D.; Nekaris, K. A. I. Large-Scale Trade in Legally Protected Marine Mollusc Shells from Java and Bali, Indonesia. *PLoS One* **2015**, *10* (12), No. e0140593.

(14) Glamuzina, B.; Tutman, P.; Glamuzina, L.; Vidović, Z.; Simonović, P.; Vilizzi, L. Quantifying Current and Future Risks of Invasiveness of Non-Native Aquatic Species in Highly Urbanised Estuarine Ecosystems—A Case Study of the River Neretva Estuary (Eastern Adriatic Sea: Croatia and Bosnia−Herzegovina). *Fish Manag Ecol* **2021**, *28* (2), 138−146.

(15) Eugene, L. R.; Singh, O. P. Degradation in Water Quality Due to Limestone Mining in East Jaintia Hills, Meghalaya, India. *Int. Res. J. Environ. Sci.* **2014**, *3*, 13−20.

(16) Iwanoff, A. Environmental impacts of deep opencast limestone mines in Laegerdorf, Northern Germany. *Mine Water Environ.* **1998**, *17*, 52−61.

(17) Ganapathi, H.; Phukan, M. *Environmental Hazards of Limestone Mining and Adaptive Practices for Environment Management Plan*; Springer, 2020; pp. 121−134

(18) Mai, M. L.; Emmett, M.; Sheikh, M. S.; Ana, C. A. S.; Schiller, L.; Fordtran, J. S. Calcium Acetate, an Effective Phosphorus Binder in Patients with Renal Failure. *Kidney Int.* **1989**, *36*, 690−695.

(19) Emmett, M.; Sirmon, M. D.; Kirkpatrick, W. G.; Nolan, C. R.; Schmitt, G. W.; Cleveland, M. V. B. Calcium Acetate Control of Serum Phosphorus in Hemodialysis Patients. *American Journal of Kidney Diseases* **1991**, *17* (5), 544−550.

(20) Pflanz, S.; Henderson, I. S.; Mcelduff, N.; Jones, M. C. Calcium Acetate versus Calcium Carbonate as Phosphate-Binding Agents in Chronic Haemodialysis. *Nephrol. Dialys. Transplant.* **1994**, *9*, 1121−1124.
(21) Palacios, C.; Cormick, G.; Hofmeyr, G. J.; Garcia-Casal, M. N.; Peña-Rosas, J. P.; Betrán, A. P. *Calcium-Fortified Foods in Public Health Programs: Considerations for Implementation. Annals of the New York Academy of Sciences*; Blackwell Publishing Inc., 2021; pp. 3−21.
(22) Abed, A. A.; Mojtahedi, A.; Lotfollahi Yaghin, M. A. Factorial Mixture Design for Properties Optimization and Modeling of Concrete Composites Incorporated with Acetates as Admixtures. *Sustainability* **2023**, *15* (13), 10608.
(23) Jeong, B.; Asce, M.; Jho, E. H.; Kim, S. H.; Nam, K. Effect of Calcium Organic Additives on the Self-Healing of Concrete Microcracks in the Presence of a New Isolate Bacillus Sp. BY1. *J. Mater. Civil Eng.* **2019**, *31*, No. 04019227.
(24) Garduño-Pineda, L.; Linares-Hernández, I.; Solache-Ríos, M. J.; Teutli-Sequeira, A.; Martínez-Miranda, V. Removal of Inorganic Chemical Species and Organic Matter from Slaughterhouse Wastewater via Calcium Acetate Synthesized from Eggshell. *J. Environ. Sci. Health A Tox Hazard Subst Environ. Eng.* **2019**, *54* (4), 295−305.
(25) Yao, Y.; Zhang, J.; Zhang, R.; Shi, Y.; An, P.; Hu, X.; Wan, Y. Optimization of Preparation of Calcium Acetate from Eggshell by Response Surface Methodology (RSM). *Food Sci. Technol.* **2022**, *42*, No. e114421.
(26) Thongkam, M.; Saelim, J.; Boonchom, B.; Seesanong, S.; Chaiseeda, K.; Laohavisuti, N.; Bunya-Atichart, K.; Boonmee, W.; Taemchuay, D. Simple and Rapid Synthesis of Calcium Acetate from Scallop Shells to Reduce Environmental Issues. *Adsorption Science and Technology* **2021**, *2021*. DOI: 10.1155/2021/6450289.
(27) Seesanong, S.; Seangarun, C.; Boonchom, B.; Laohavisuti, N.; Thompho, S.; Boonmee, W.; Mongkol, S.; Rungrojchaipon, P. Bio-Green Synthesis of Calcium Acetate from Oyster Shell Waste at Low Cost and Reducing the Emission of Greenhouse Gases. *Sustainable Environment Research* **2023**, *33* (1). DOI: 10.1186/s42834-023-00187-6.
(28) Pînzaru, S. C.; Popl̆acean, I.-C.; Maškarić, K.; Dumitru, D.-A.; Barbu-Tudoran, L.; Tămaş, T.-L.; Nekvapil, F.; Neculai, B. Raman Technology for Process Control: Waste Shell Demineralization for Producing Transparent Polymer Foils Reinforced with Natural Antioxidants and Calcium Acetate By-Products. *Processes* **2024**, *12* (4), 832.
(29) Musumeci, A. W.; Frost, R. L.; Waclawik, E. R. A Spectroscopic Study of the Mineral Paceite (Calcium Acetate). *Spectrochim Acta A Mol. Biomol Spectrosc* **2007**, *67* (3−4), 649−661.
(30) Panzer, J. Nature of Calcium Acetate. *J. Chem. Eng. Data* **1962**, *7* (1), 140−142.
(31) Bette, S.; Stelzner, J.; Eggert, G.; Schleid, T.; Matveeva, G.; Kolb, U.; Dinnebier, R. E. Corrosion of Heritage Objects: Collagen-Like Triple Helix Found in the Calcium Acetate Hemihydrate Crystal Structure. *Angewandte Chemie - International Edition* **2020**, *59* (24), 9438−9442.
(32) Bette, S.; Müller, M. X.; Eggert, G.; Schleid, T.; Dinnebier, R. E. Efflorescence on Calcareous Objects in Museums: Crystallisation, Phase Characterisation and Crystal Structures of Calcium Acetate Formate Phases. *Dalton Transactions* **2019**, *48* (42), 16062−16073.

https://doi.org/10.1021/acsomega.4c04138
ACS Omega 2024, 9, 37086−37093